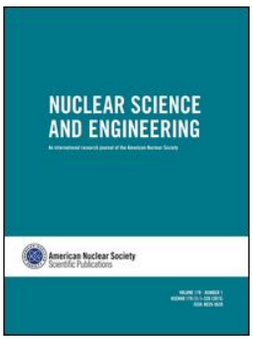

Nuclear Science and Engineering

ISSN: 0029-5639 (Print) 1943-748X (Online) Journal homepage: http://www.tandfonline.com/loi/unse20

An Efficient Multidimensional Numerical Method for the Thermal-Hydraulic Analysis of Nuclear Reactor Cores

Robert E. Masterson & Lothar Wolf

To cite this article: Robert E. Masterson & Lothar Wolf (1977) An Efficient Multidimensional Numerical Method for the Thermal-Hydraulic Analysis of Nuclear Reactor Cores, Nuclear Science and Engineering, 64:1, 222-236, DOI: 10.13182/NSE77-A27093

To link to this article: http://dx.doi.org/10.13182/NSE77-A27093

Published online: 13 May 2017.

NUCLEAR SCIENCE AND ENGINEERING: 64, 222-236 (1977)

An Efficient Multidimensional Numerical Method for the Thermal-Hydraulic Analysis of Nuclear Reactor Cores

Robert E. Masterson and Lothar Wolf

Massachusetts Institute of Technology, Department of Nuclear Engineering
Cambridge, Massachusetts 02139

Received January 13, 1977
Revised February 14, 1977

A new numerical method is presented for the steady-state and transient, two-phase, lumped parameter thermal-hydraulic analysis of the fluid flow distributions in fuel pin bundles and nuclear reactor cores. The method uses the same physical model as the COBRA-IIIC code, but is based on the alternative numerical concept of generating a system of semi-implicit difference equations for the pressure field using a spatial differencing scheme that is different from the schemes previously used by subchannel analysis codes. The flow and enthalpy distributions in the lattice are found by marching downstream several times in succession between adjacent computational planes and by combining the computed pressure fields from these planes together into a composite pressure field, which is then used as the driving force for the cross-flow distribution in a reformulated form of the transverse momentum equation. The method is extremely efficient from a computational point of view and is compatible with a variety of iterative techniques, because the coefficient matrices governing the pressure field can be shown to have diagonal dominance and a simple, predictable band structure for a variety of subchannel numbering schemes.

The numerical method has been integrated into the computational framework of the COBRA-IIIC code, and a new computer code has been written called COBRA-IIIP/MIT (P for a pressure solution). The code is considerably faster and more powerful than many other reactor thermal-hydraulic analysis codes and has the capability of solving extremely large and complex problems with great speed. Calculations are presented in this paper in which the results of the new code and the numerical method on which it is based are compared to those of COBRA-IIIC.

I. INTRODUCTION

In recent years, many attempts have been made to develop numerical methods for solving the set of fluid conservation equations that characterizes the steady-state and transient thermal-hydraulic performance of fuel pin bundles and nuclear reactor cores. These equations are usually developed from a control volume approach before they are cast into a form more suitable for digital computer analysis. The purpose of this paper is to present a new numerical method for solving these equations that is considerably faster and more efficient than previous methods used to analyze operational reactor conditions.

An excellent review of the state-of-the-art of thermal-hydraulic analysis codes developed over the last decade has been given by Weisman and Bowring.[1] Most of these codes simplify the solution of the conservation equations by dividing the lattice into a number of computational cells having the same size and shape and by using an initial value approach to alleviate the numerical difficulties associated with obtaining a solution to the true boundary value problem. In cases where all the cells are used to represent individual subchannels, this analysis is referred to as subchannel analysis. These simplifications have enabled subchannel analysis codes to handle fuel pin

[1] J. WEISMAN and R. W. BOWRING, *Nucl. Sci. Eng.*, **57**, 255 (1975).

bundles having as many as 37 rods,[2] although the most widely used and acknowledged code, e.g., COBRA-IIIC (Ref. 3), has generally been used to analyze problems having smaller numbers of computational cells. Attempts to extend the COBRA-IIIC code to larger and more complex problems have generally failed to yield satisfactory results due to the fact that it has not been possible to analyze these problems economically without major changes in the structure or the logic of the solution scheme used by the code.[4]

Progress has recently been made to overcome this deficiency by reinterpreting the concept of the subchannel and smearing several subchannels together to identify larger computational cells. This approach permits detailed subchannel calculations to be performed with a reasonable number of cells, while maintaining the character of the physical interaction between the subchannels and the rest of the assembly. Unfortunately, this concept requires the derivation of transport coefficients to describe the interchange of mass, energy, and momentum between regions having different sizes, thermal-hydraulic properties, and geometrical shapes.[5,6]

The COBRA-IIIC/MIT code[7,8] is an improved version of the original COBRA-IIIC code that takes advantage of the sparsity of the cross-flow coefficient matrix and a more efficient coding scheme to reduce the running time to more acceptable levels. The COBRA-IIIC/MIT code uses the same physical and mathematical models as COBRA-IIIC to compute the flow and enthalpy distributions, and gives exactly the same results for the classes of problems to which it can be applied. The COBRA-IIIC/MIT code has a reasonable running time and has the capability of handling complex problems having more than 100 computational cells.

Whereas all of the aforementioned codes are applicable to operational reactor conditions, the recently developed COBRA-IV-I code[9] represents significant progress in the field of accident analysis because it solves the conservation equations as a true boundary value problem using an adaptation of the MAC method[10] to the control volume approach developed by Rowe.[3] The COBRA-IV-I code comprises all the features of a true benchmark code and can consider the effects of severe flow blockages, coolant expulsions, flow reversals, and recirculations. The code also contains a vastly improved version of the COBRA-IIIC code in which an iterative solution scheme for the cross-flow distribution is used to reduce the execution time to levels similar to those obtained with COBRA-IIIC/MIT.

Based on these observations, the primary objectives of the present work are:

1. to furnish a more efficient computational tool for analyzing any given lattice containing a very large number of computational cells during operational reactor conditions
2. to ensure stability and effective convergence of the method
3. to improve the representation and interpretation of the cross-flow distributions
4. to provide a computational tool of greater flexibility by providing both iterative and direct methods for determining the cross-flow distribution.

II. TOPOLOGY

The following discussion is concerned primarily with the development of a numerical method for predicting the flow and enthalpy distributions in square arrays of fuel pins and fuel pin assemblies such as those shown in Figs. 1 through 4. In this discussion, a computational cell is used to represent either a subchannel, a smeared group of subchannels, an assembly, or a smeared cluster of assemblies. The lattice can consist of cells having the same size and shape or mixture of more complex cells having a variety of different

[2]K. G. BECKER and P. PERSSON, "Predictions of Burnout-Conditions for Full-Scale 36 Rod Bundles with Uniform and Non-Uniform Heat Flux Employing the COBRA Subchannel Analysis and the Becker Burnout Correlations," Paper D-2, European Two-Phase Flow Mtg., Milan, Italy (June 1970).

[3]D. S. ROWE, "COBRA-IIIC: A Digital Computer Program for Steady State and Transient Thermal Analysis of Rod Bundle Nuclear Fuel Elements," BNWL-1695, Battelle-Pacific Northwest Laboratories (1973).

[4]H. C. HERBIN, "Analysis of Operating Data Related to Power and Flow Distributions in a PWR," NED Thesis, Massachusetts Institute of Technology (June 1974).

[5]P. MORENO, "Thermal/Hydraulic Analysis Methods for PWR's," NED Thesis, Massachusetts Institute of Technology (May 1976).

[6]C. CHIU, "Two-Dimensional Transport Coefficients for the PWR's Thermal/Hydraulic Analysis," BS Thesis, Massachusetts Institute of Technology (May 1976).

[7]R. BOWRING and P. MORENO, "COBRA-IIIC/MIT Computer Code Manual," Massachusetts Institute of Technology (1976), unpublished.

[8]Massachusetts Institute of Technology, "MEKIN: MIT-EPRI Nuclear Reactor Core Kinetics Code," EPRI-Research Project 227, Electric Power Research Institute (1975).

[9]C. L. WHEELER et al., "COBRA-IV-I: An Interim Version of COBRA for Thermal-Hydraulic Analysis of Rod Bundle Nuclear Fuel Elements and Cores," BNWL-1962, Battelle-Pacific Northwest Laboratories (1976).

[10]C. W. STEWART and D. S. ROWE, *Trans. Am. Nucl. Soc.*, **24**, 178 (1976).

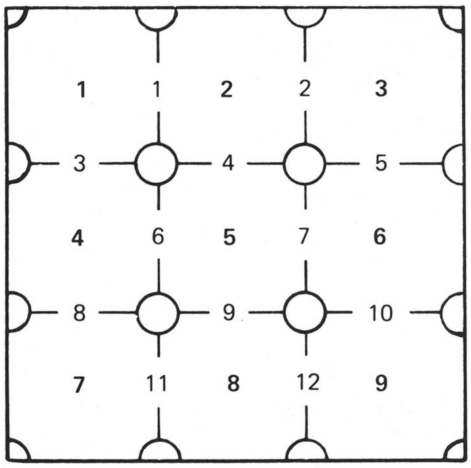

Fig. 1. A consistent subchannel numbering scheme.

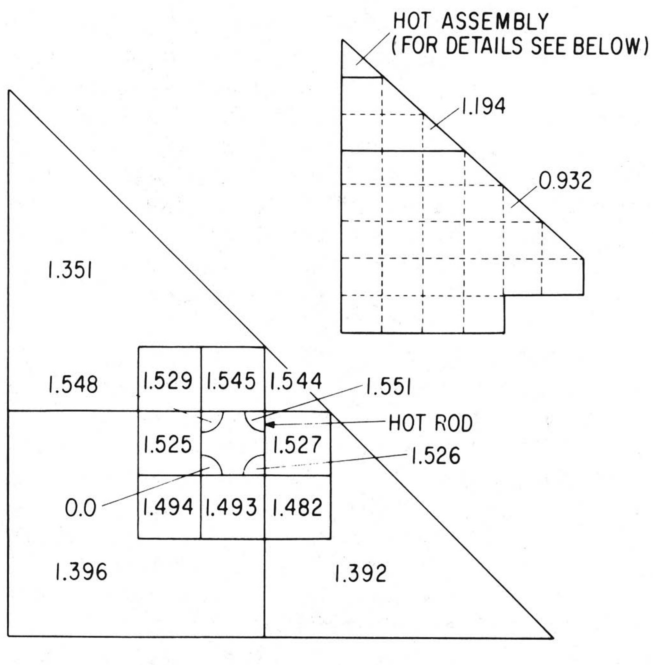

Fig. 2. Sample problem I for a mixed-lattice calculation $\frac{1}{8}$ full-core symmetry scheme including hottest subchannel in hot assembly (power is normalized to 1.0).

sizes and shapes. Examples of these configurations of cells are shown in Figs. 1 and 2, respectively. The arrangement of cells shown in Fig. 2 is often preferable to the arrangements used in fixed lattice codes such as the THINC-CHAIN (Refs. 11 and 12) and LYNX (Refs. 13 and 14) codes because it allows the user to specify whatever physical detail he feels is necessary to describe the characteristics of the problem on hand. However, the size and shape of these cells and their location in the lattice may have some effect upon the efficiency of the method used to determine the flow and enthalpy fields. Finally, it should be recognized that a very detailed spatial modeling scheme should be used to verify the validity of mixed-lattice calculations, particularly if the concept of a mixed lattice is to be used successfully to model specific regions of interest within a reactor during the course of a transient.

III. MATHEMATICAL FORMULATION

Due to the widespread acceptance and use of the COBRA-IIIC code, a considerable amount of the physical and mathematical formalism employed by the code is also used as the basis for the numerical method to be developed here. This essentially means that the same basic set of governing conservation equations is considered and that the same marching-type of solution procedure used for the initial value problem is retained in space and time. The objective of the method to be proposed is to solve the fluid conservation equations as efficiently as possible, so that much larger and more complex problems can be handled within the limits of existing computational capacity.

III.A. Basic Assumptions

With these points in mind, the assumptions of primary importance to the following development are:

1. A lumped-parameter approach is valid.
2. Sonic velocity propagation is ignored.
3. The diversion cross flow is small compared to the axial mass flow.
4. Flow reversals, recirculating flows, and coolant expulsions are not considered.

III.B. Governing Set of Equations

By using the control volume approach described in Ref. 3 the equations for the conservation of mass, energy, and momentum can be written as

[11]H. CHELEMER, J. WEISMAN, and L. S. TONG, *Nucl. Eng. Design*, **21**, 35 (1972).

[12]P. T. CHU, H. CHELEMER, and L. E. HOCHREITER, "THINC-IV, An Improved Program for Thermal-Hydraulic Analysis of Rod Bundle Cores," WCAP-7956, Westinghouse Electric Corporation (1973).

[13]B. R. HAO and J. M. ALCORN, "LYNX1–Reactor Fuel Assembly Thermal-Hydraulic Analysis Code," BAW-10129, Babcock and Wilcox Company (1976).

[14]B. R. HOPPER and J. R. GLOUDEMANS, "LYNX2–Subchannel Thermal-Hydraulic Analysis Program," BAW-10130, Babcock and Wilcox Company (1976).

Continuity:

$$[A]\left\{\frac{\partial P}{\partial t}\right\} + \left\{\frac{\partial m}{\partial x}\right\} = -[S]^T\{w\} \quad , \tag{1}$$

Energy:

$$\left\{\frac{1}{\ddot{u}}\frac{\partial h}{\partial t}\right\} + \left\{\frac{\partial h}{\partial x}\right\} = \left[\frac{1}{m}\right]\{Q\} - \left[\frac{1}{m}\right][S]^T[\Delta h]\{w'\} - \left[\frac{1}{m}\right][S]^T[\Delta t]\{c\} + \left[\frac{1}{m}\right]\left[[h][S]^T - [S]^T[h^*]\right]\{w\} \quad , \tag{2}$$

Axial Momentum:

$$\left[\frac{1}{A}\right]\left\{\frac{\partial m}{\partial t}\right\} - \left\{2u\frac{\partial \rho}{\partial t}\right\} + \left\{\frac{\partial P}{\partial x}\right\} = \{a'\} + \left[\frac{1}{A}\right]\left[[2u][S]^T - [S]^T[u^*]\right]\{w\} \quad , \tag{3}$$

where the components of the pressure drop due to frictional forces, gravitational forces, and the effects of turbulent mixing are given by

$$\{a'\} = -\left\{\left(\frac{m}{A}\right)^2\left[\frac{vf\phi}{2D} + \frac{Kv'}{2\Delta x} + A\frac{\partial(v'/A)}{\partial x}\right] + \rho g\cos\phi\right\} - f_\tau\left[\frac{1}{A}\right][S]^T[\Delta u]\{w'\} \quad . \tag{4}$$

Transverse interactions are taken into account by means of the transverse momentum equation developed for the COBRA-IIIC code:

Transverse Momentum:

$$\left\{\frac{\partial w}{\partial t}\right\} + \left\{\frac{\partial(u^*w)}{\partial x}\right\} + \left(\frac{s}{l}\right)[C]\{w\} = \left(\frac{s}{l}\right)[S]\{P\} \quad . \tag{5}$$

This set of equations is closed by defining an additional equation for the physical state of the coolant, and empirical correlations for turbulent mixing coefficients, friction factors, and heat transfer coefficients. For convenience, the same nomenclature and notation used in Ref. 3 are also used here. Consequently, the reader is referred to Ref. 3 for more detailed information about the definition and derivation of the individual terms.

The foregoing conservation equations must be converted into a system of difference equations before they can be solved by numerical means. Taking a first-order backward differencing scheme for the spatial and temporal derivatives allows the conservation equations to be written as

Continuity:

$$[A_j]\left\{\frac{\rho_j - \bar{\rho}_j}{\Delta t}\right\} + \left\{\frac{m_j - m_{j-1}}{\Delta x}\right\} = -[S]^T\{w_j\} \quad , \tag{6}$$

Energy

$$\left\{\frac{1}{\ddot{u}_j}\right\}\left\{\frac{h_j - \bar{h}_j}{\Delta t}\right\} + \left\{\frac{h_j - h_{j-1}}{\Delta x}\right\} = \{m_j\}^{-1}\left\{\{Q_{j-1/2}\} - [S][\Delta h_{j-1}]\{w'_{j-1}\} - [S]^T[\Delta t_{j-1}][c_{j-1}]\right\} + \{m_j\}^{-1} \times \left[[h_{j-1}][S]^T - [S]^T[h^*_{j-1}]\right] . \tag{7}$$

Axial Momentum:

$$[A_j]^{-1}\left\{\frac{m_j - \bar{m}_j}{\Delta t}\right\} - [2u_j]\left\{\frac{\rho_j - \bar{\rho}_j}{\Delta t}\right\} + \left\{\frac{P_j - P_{j-1}}{\Delta x}\right\} = \{a'_{j-1}\} + [A_j]^{-1}\left[[2u_j][S]^T - [S]^T[u^*_j]\right]\{w_j\} \quad . \tag{8}$$

In this differencing scheme, each control volume is bounded by two adjacent control volumes in the axial direction, and the interchange of mass, energy, and momentum is allowed to occur between adjacent computational cells in the transverse plane. It can easily be seen that this differencing scheme has a truncation error of $0(\Delta x,\Delta t)$. Although many other differencing schemes are possible, this scheme is the only one that is considered here. Finally, it must be understood that the transverse momentum equation has been excluded from the preceding discussion. This equation is now considered in more detail since a better knowledge of its structural properties, as well as the differencing schemes that can be applied to it, is necessary to gain a more comprehensive understanding of the proposed method.

IV. SOLUTION TECHNIQUES

IV.A. Development of a New Spatial Differencing Scheme for the Transverse Momentum Equation

The purpose of the transverse momentum equation is to couple the computational cells together so that pressure gradients generated by the axial momentum equation can be used as the driving forces for the transport of mass, energy, and momentum between computational cells in the transverse plane. The purpose of this section is to present a new spatial differencing scheme for the transverse momentum equation, which will be used as the basis for the development of the newly proposed method. The idea of the differencing scheme is to split the pressure vector and all the other forcing terms that drive the cross flow in the transverse momentum equation into a sum of spatially implicit and explicit parts. By introducing the weighting function, θ, having an

arbitrary value between 0.0 and 1.0, the pressure vector $\{P\}$ and the cross-flow resistance terms $[C]\{w\}$ in Eq. (5) can be written as

$$\{P\} = \theta\{P_j\} + (1 - \theta)\{P_{j-1}\} \tag{9}$$

$$[C]\{w\} = \theta[C_j]\{w_j\} + (1 - \theta)[C_{j-1}]\{w_{j-1}\} \ , \tag{10}$$

where

$$0.0 \leq \theta \leq 1.0 \ .$$

By introducing these two equations into the finite difference form of Eq. (5),

$$\left\{\frac{w_j - \overline{w}_j}{\Delta t}\right\} + \left\{\frac{u_j w_j - u^*_{j-1} w_{j-1}}{\Delta x}\right\} + \left(\frac{s}{l}\right)[C]\{w\} = \left(\frac{s}{l}\right)[S]\{P\} \ , \tag{11}$$

it is possible to write the transverse momentum equation more generally as

$$\left\{\frac{w_j - \overline{w}_j}{\Delta t}\right\} + \left\{\frac{u^*_j w_j - u^*_{j-1} w_{j-1}}{\Delta x}\right\} + \left(\frac{s}{l}\right) \times \left\{\theta[C_j]\{w_j\} + (1 - \theta)[C_{j-1}]\{w_{j-1}\}\right\} = \left(\frac{s}{l}\right)[S]\left\{\theta\{P_j\} + (1 - \theta)\{P_{j-1}\}\right\} \ , \tag{12}$$

where the significance of the proposed differencing scheme can be seen by examining the form of the transverse momentum equation for various values of θ; e.g., by setting θ equal to 0.0, $\frac{1}{2}$, and 1.0, respectively,

$\theta = 0.0$:

$$\left\{\frac{w_j - \overline{w}_j}{\Delta t}\right\} + \left\{\frac{u^*_j w_j - u^*_{j-1} w_{j-1}}{\Delta x}\right\} + \left(\frac{s}{l}\right)[C_{j-1}]\{w_{j-1}\} = \left(\frac{s}{l}\right)[S]\{P_{j-1}\} \ , \tag{13}$$

$\theta = \frac{1}{2}$:

$$\left\{\frac{w_j - \overline{w}_j}{\Delta t}\right\} + \left\{\frac{u^*_j w_j - u^*_{j-1} w_{j-1}}{\Delta x}\right\} + \left(\frac{s}{l}\right)\left\{\frac{[C_j]\{w_j\} + [C_{j-1}]\{w_{j-1}\}}{2}\right\} = \left(\frac{s}{l}\right)[S] \times \left\{\frac{\{P_j\} + \{P_{j-1}\}}{2}\right\} \ , \tag{14}$$

$\theta = 1.0$:

$$\left\{\frac{w_j - \overline{w}_j}{\Delta t}\right\} + \left\{\frac{u^*_j w_j - u^*_{j-1} w_{j-1}}{\Delta x}\right\} + \left(\frac{s}{l}\right)[C_j]\{w_j\} = \left(\frac{s}{l}\right)[S]\{P_j\} \ . \tag{15}$$

Thus, it can be seen that an approach has been developed that allows the cross-flow distribution to be driven by any combination of the pressure fields that exist at the top and the bottom of each plane of computational cells. By choosing a value for θ, the pressure fields from adjacent axial levels can be blended together in a manner that allows the degree of coupling of the transverse and axial momentum equations to be a function of the problem being solved. This blending of the pressure fields tends to eliminate sudden changes in the transverse cross-flow distribution caused by discontinuities resulting from the application of the correlations for the pressure gradients at the interface between flow regimes, and allows a more general physical model to be used to describe the transfer of momentum between the computational cells.

IV.B. Detailed Development of the Method

Using the aforementioned difference equations as the starting point for the development of the proposed method, it should be noted that it is desirable to construct a procedure that simultaneously guarantees the conservation of mass and momentum at each axial elevation of the core at each instant of time. This condition can be satisfied by combining the continuity equation, Eq. (6), together with the axial momentum equation, Eq. (8), to explicitly eliminate the time-dependent density term, $\{\partial\rho/\partial t\}$. The result of this substitution is a set of matrix equations of the form

$$[A_j]^{-1}\left\{\frac{m_j - \overline{m}_j}{\Delta t}\right\} + [2u_j][A_j]^{-1}\left\{\frac{m_j - m_{j-1}}{\Delta x}\right\} + [2u_j][A_j]^{-1}[S]^T\{w_j\} + \left\{\frac{P_j - P_{j-1}}{\Delta x}\right\} = \{a'_{j-1}\} + [A_j]^{-1}[2u_j][S]^T\{w_j\} - [A_j]^{-1}[S]^T[u^*_j]\{w_j\} \ . \tag{16}$$

Since $[A_j]$, $[A_j]^{-1}$, and $[u_j]$ are diagonal matrices, Eq. (16) can also be written as

$$[A_j]^{-1}\left\{\frac{m_j - \overline{m}_j}{\Delta t}\right\} + [2u_j][A_j]^{-1}\left\{\frac{m_j - m_{j-1}}{\Delta x}\right\} + \left\{\frac{P_j - P_{j-1}}{\Delta x}\right\} = \{a'_{j-1}\} - [A_j]^{-1}[S]^T[u^*_j]\{w_j\} \ . \tag{17}$$

The transverse momentum equation, Eq. (12), is then solved for the cross-flow distribution as function of the pressure distribution, giving

$$\left[\frac{1}{\Delta t}+\frac{u_j^*}{\Delta x}+\left(\frac{s}{l}\right)\theta[C_j]\right]\{w_j\}=\left\{\frac{\overline{w}_j}{\Delta t}\right\}+\left\{\frac{u_{j-1}^* w_{j-1}}{\Delta x}\right\}+\left(\frac{s}{l}\right)(\theta-1)[C_{j-1}]\{w_{j-1}\}+\left(\frac{s}{l}\right)[S]\times\left\{\theta\{P_j\}+(1-\theta)\{P_{j-1}\}\right\} \quad (18)$$

This system of equations can also be written in the form

$$\{w_j\}=[D_j]^{-1}\left\{\left\{\frac{\overline{w}_j}{\Delta t}\right\}+\left\{\frac{u_{j-1}^* w_{j-1}}{\Delta x}\right\}+\left(\frac{s}{l}\right)(\theta-1)[C_{j-1}]\{w_{j-1}\}\right\}+\left(\frac{s}{l}\right)[D_j]^{-1}[S]\times\left\{\theta\{P_j\}+(1-\theta)\{P_{j-1}\}\right\} , \quad (19)$$

where

$$[D_j]^{-1}=\left[\frac{1}{\Delta t}+\frac{u_j^*}{\Delta x}+\left(\frac{s}{l}\right)\theta[C_j]\right]^{-1} . \quad (20)$$

Substituting Eq. (19) into Eq. (17) to explicitly eliminate the cross-flow distribution results in the following system of fundamental equations for the pressure field

$$[A_j]^{-1}\left\{\frac{m_j-\overline{m}_j}{\Delta t}\right\}+[2u_j][A_j]^{-1}\left\{\frac{m_j-m_{j-1}}{\Delta x}\right\}+\left\{\frac{P_j-P_{j-1}}{\Delta x}\right\}=\{a'_{j-1}\}-[A_j]^{-1}[S]^T[u_j^*][D_j]^{-1}\times\left\{\left\{\frac{\overline{w}_j}{\Delta t}\right\}+\left\{\frac{u_{j-1}^* w_{j-1}}{\Delta x}\right\}+\left(\frac{s}{l}\right)(\theta-1)[C_{j-1}]\{w_{j-1}\}\right\}-\left(\frac{s}{l}\right)[A_j]^{-1}[S]^T[u_j^*]\times[D_j]^{-1}[S]\left\{\theta\{P_j\}+(1-\theta)\{P_{j-1}\}\right\} . \quad (21)$$

Additional algebraic manipulation allows these equations to be written more elegantly as

$$[I+\theta M_j]\{P_j\}=[I-(1-\theta)M_j]\{P_{j-1}\}+\{b_j\} , \quad (22)$$

where

$$[M_j]=\Delta x\left(\frac{s}{l}\right)[A_j]^{-1}[S]^T[u_j^*][D_j]^{-1}[S] , \quad (23)$$

where $[I]$ is the identity matrix, and the vector $\{b_j\}$ is given by

$$\{b_j\}=\Delta x\{a'_{j-1}\}-\left(\frac{\Delta x}{\Delta t}\right)[A_j]^{-1}\{m_j-\overline{m}_j\}-[A_j]^{-1}\times[2u_j]\{m_j-m_{j-1}\}-\Delta x[A_j]^{-1}[S]^T[u_j^*]\times[D_j]^{-1}[S]\left\{\frac{\overline{w}_j}{\Delta t}+\frac{u_{j-1}^* w_{j-1}}{\Delta x}+\left(\frac{s}{l}\right)(\theta-1)[C_{j-1}]\{w_{j-1}\}\right\} . \quad (24)$$

Note that $\{b_j\}$ is a source vector containing all terms that contribute to the axial pressure gradient, including those due to frictional forces, gravitational forces, to the cross-flow distribution that has existed at previous points in space and time, and to the spatial and temporal acceleration of the flow. In spite of the seemingly complex structure of this vector, it should be noted that it contains only one entry from each computational cell. Finally, the value of $\{m_j\}$ in Eq. (21) is unknown, but can be initially estimated and undated through iteration. The procedure by which this is done is assumed to be exactly the same as that used by COBRA-IIIC.

IV.C. Detailed Discussion of the Difference Equations

To more clearly comprehend the consequences of the procedure that has been proposed, it is helpful to write Eq. (22) as

$$\{P_j\}=[I+\theta M_j]^{-1}[I-(1-\theta)M_j]\{P_{j-1}\}+[I+\theta M_j]^{-1}\{b_j\} , \quad (25)$$

and to examine the structure of the matrix equations governing the pressure field $\{P_j\}$ for various values of θ. Setting $\theta = 0.0$, $\frac{1}{2}$, and 1.0 allows Eq. (25) to be written in the following three forms:

$\theta = 0.0$:

$$\{P_j\}=[I-M_j]\{P_{j-1}\}+\{b_j\} . \quad (26)$$

$\theta = \frac{1}{2}$:

$$\{P_j\}=\left[I+\frac{M_j}{2}\right]^{-1}\left[I-\frac{M_j}{2}\right]\{P_{j-1}\}+\left[I+\frac{M_j}{2}\right]^{-1}\{b_j\} , \quad (27)$$

$\theta = 1.0$:

$$\{P_j\}=[I+M_j]^{-1}\{P_{j-1}\}+[I+M_j]^{-1}\{b_j\} . \quad (28)$$

These equations demonstrate that a direct relationship exists between the form of the equations for the pressure field and the forces used to drive the cross-flow distribution between the computational cells in the transverse plane. Setting $\theta = 0.0$ allows the cross-flow distribution to be driven by the pressure field that exists at the bottom of each plane of computational cells. From Eq. (26), it can be seen that this results in a differencing scheme that is spatially explicit but temporally implicit. Choosing $\theta = 1.0$ means that the cross-flow distribution is governed by the pressure field that exists at the top of each plane of computational cells. This, in turn, is numerically equivalent to requiring that the system of equations to be solved for the pressure field is fully implicit as denoted by Eq. (28). Finally, by setting $\theta = \frac{1}{2}$, Eq. (27) shows that it is possible to generate a system of equations where the cross-flow distribution is driven by the average of the pressure distributions that exist at the top and the bottom of each plane of computational cells. In this specific case, the difference equations are temporally implicit but have a spatial component whose structure is analogous to that of the Crank-Nicholson method. It should be noted that other values of θ lead to other spatial differencing schemes, and in fact, a whole spectrum of these schemes can be generated from Eq. (25) by selecting other values of θ. Finally, it should be recognized that it is theoretically possible to select an optimum spatial differencing scheme that most closely meets the requirements of the specific problem being solved.

IV.D. Derivation of the Cross-Flow Distribution

When pressure gradients develop between the computational cells at a given axial elevation, the flow field in the lattice becomes perturbed and a cross-flow distribution is set up to equalize imbalances in the radial pressure field. To account for the effects of the cross-flow distribution on the interchange of mass and momentum between the computational cells, the cross-flow distribution must first be found from the transverse momentum equation, Eq. (5). The pressure vector used to drive the cross-flow distribution in this equation is found by blending the pressure field computed from Eq. (25) together with the pressure field from the previous axial level to form a composite pressure field, Eq. (9), as the numerical scheme sweeps downstream. The cross-flow distribution at successive axial steps is then found from Eq. (12) by rewriting it as

$$\{w_j\} = [D_j]^{-1}\left\{\left\{\frac{\overline{w}_j}{\Delta t}\right\} + \left\{\frac{u_j^* w_{j-1}}{\Delta x}\right\} + \left(\frac{s}{l}\right)(\theta - 1)[C_{j-1}]\{w_{j-1}\}\right\} + \left(\frac{s}{l}\right)[D_j]^{-1}[S]\left\{\theta\{P_j\} + (1-\theta)\{P_{j-1}\}\right\}, \tag{29}$$

where $[D_j]^{-1}$ is the diagonal matrix defined by Eq. (20). This additional step requires very little computational effort since the inverse of $[D_j]$ can be found by inspection. Finally, it should be recognized that no assumption has been made so far with regard to θ; i.e., θ can still assume an arbitrary value between 0.0 and 1.0.

IV.E. A Comparison to the Numerical Method Used by COBRA-IIIC

To more clearly comprehend the capabilities of the method that has been developed, it is instructive to compare its features to those of the method used by COBRA-IIIC.

The starting point for the comparison is the equation used to compute the cross-flow distribution in the COBRA-IIIC code,

$$[M_j]_c\{w_j\}_c = \{b_j\}_c , \tag{30}$$

where

$$[M_j]_c = \left[\frac{1}{\Delta t}\right] + \left[\frac{u_j^*}{\Delta x}\right] + \left(\frac{s}{l}\right)[C_j] + \Delta x\left(\frac{s}{l}\right)[S][A_j]^{-1} \times \left[[2u_j][S]^T - [S]^T[u_j^*]\right] \tag{31}$$

is the coefficient matrix that drives the transverse flow field,

$$\{b_j\}_c = \left\{\frac{\overline{w}_j}{\Delta t}\right\} + \left\{\frac{u_{j-1}^* w_{j-1}}{\Delta x}\right\} + \Delta x\left(\frac{s}{l}\right)[S] \times \left\{\{a_j'\} - [A_j]^{-1}\left\{\frac{m_j - \overline{m}_j}{\Delta t}\right\} + [2u_j]\left\{\frac{\rho_j - \overline{\rho}_j}{\Delta t}\right\}\right\} \tag{32}$$

is the source vector that generates the transverse flow field, and where the subscript c refers to the fact that these equations are used by the COBRA-IIIC code.

The comparison of the two methods is begun by examining the structure of the coefficient matrix used by each method and the consequence of these structural properties from a numerical point of view. A more detailed discussion of the meaning of the terms to be used is given in Ref. 3.

The analysis of Eq. (30) starts by realizing that $[A_j]$, $[u_j]$, and $[u_j^*]$ are diagonal matrices. With this simplification, it is possible to write the cross-flow coefficient matrix more generally as

$$[M_j]_c = [C_1][I] + [C_2][S][S]^T \quad , \tag{33}$$

where $[C_1]$ and $[C_2]$ are matrices containing parameters that are problem dependent, $[I]$ is the identity matrix, and $[S]$ and $[S]^T$ are "geometrical connection matrices" whose purpose is to maintain a consistent ordering scheme between the cells used to define the topology of the lattice and boundaries used to define interactions between adjacent cells. Equation (33) shows that the structure of the cross-flow coefficient matrix is determined primarily by the order of multiplication of $[S]$ and $[S]^T$ for the simple subchannel numbering scheme shown in Fig. 1.

In these equations, the number of cross flows is indicated by the symbol NF and the number of nodes at which the pressure is to be found by the symbol NP. Here, as in COBRA-IIIC, the cross flow is considered to be positive when the dominant direction of fluid flow is from cell i to cell j, where i is less than j. From Eqs. (34) and (35), it can be seen that $[S]$ and $[S]^T$ are generally rectangular matrices rather than square matrices, since they represent a topological situation in which there are considerably more boundaries than computational cells. Thus, $[S]$ is an $NP \times NF$ matrix whereas its transpose, $[S]^T$, is an $NF \times NP$ matrix. Taking the product of $[S]$ and $[S]^T$ for the subchannel numbering scheme shown in Fig. 1 results in an $NF \times NF$ matrix given by Eq. (36):

$$[S] = \overset{\longleftarrow NP \longrightarrow}{\begin{bmatrix} 1 & -1 & 0 & 0 & 0 & 0 & 0 & 0 & 0 \\ 0 & 1 & -1 & 0 & 0 & 0 & 0 & 0 & 0 \\ 1 & 0 & 0 & -1 & 0 & 0 & 0 & 0 & 0 \\ 0 & 1 & 0 & 0 & -1 & 0 & 0 & 0 & 0 \\ 0 & 0 & 1 & 0 & 0 & -1 & 0 & 0 & 0 \\ 0 & 0 & 0 & 1 & -1 & 0 & 0 & 0 & 0 \\ 0 & 0 & 0 & 0 & 1 & -1 & 0 & 0 & 0 \\ 0 & 0 & 0 & 1 & 0 & 0 & -1 & 0 & 0 \\ 0 & 0 & 0 & 0 & 1 & 0 & 0 & -1 & 0 \\ 0 & 0 & 0 & 0 & 0 & 1 & 0 & 0 & -1 \\ 0 & 0 & 0 & 0 & 0 & 0 & 1 & -1 & 0 \\ 0 & 0 & 0 & 0 & 0 & 0 & 0 & 1 & -1 \end{bmatrix}} \begin{matrix} \\ \\ \\ \\ \\ \\ \\ \\ \\ \\ \\ \\ \end{matrix} \overset{\uparrow}{\underset{\downarrow}{NF}} \tag{34}$$

$$[S]^T = \overset{\longleftarrow NF \longrightarrow}{\begin{bmatrix} 1 & 0 & 1 & 0 & 0 & 0 & 0 & 0 & 0 & 0 & 0 & 0 \\ -1 & 1 & 0 & 1 & 0 & 0 & 0 & 0 & 0 & 0 & 0 & 0 \\ 0 & -1 & 0 & 0 & 1 & 0 & 0 & 0 & 0 & 0 & 0 & 0 \\ 0 & 0 & -1 & 0 & 0 & 1 & 0 & 1 & 0 & 0 & 0 & 0 \\ 0 & 0 & 0 & -1 & 0 & -1 & 1 & 0 & 1 & 0 & 0 & 0 \\ 0 & 0 & 0 & 0 & -1 & 0 & -1 & 0 & 0 & 1 & 0 & 0 \\ 0 & 0 & 0 & 0 & 0 & 0 & 0 & -1 & 0 & 0 & 1 & 0 \\ 0 & 0 & 0 & 0 & 0 & 0 & 0 & 0 & -1 & 0 & -1 & 1 \\ 0 & 0 & 0 & 0 & 0 & 0 & 0 & 0 & 0 & -1 & 0 & -1 \end{bmatrix}} \begin{matrix} \\ \\ \\ \\ \\ \\ \\ \\ \\ \\ \\ \\ \end{matrix} \overset{\uparrow}{\underset{\downarrow}{NP}} \tag{35}$$

$$[S][S]^T = \overset{\longleftarrow NF \longrightarrow}{\begin{bmatrix} 2 & -1 & 1 & -1 & 0 & 0 & 0 & 0 & 0 & 0 & 0 & 0 \\ -1 & 2 & 0 & 1 & -1 & 0 & 0 & 0 & 0 & 0 & 0 & 0 \\ 1 & 0 & 2 & 0 & 0 & -1 & 0 & -1 & 0 & 0 & 0 & 0 \\ -1 & 1 & 0 & 2 & 0 & 1 & -1 & 0 & -1 & 0 & 0 & 0 \\ 0 & -1 & 0 & 0 & 2 & 0 & 1 & 0 & 0 & -1 & 0 & 0 \\ 0 & 0 & -1 & 1 & 0 & 2 & -1 & 1 & -1 & 0 & 0 & 0 \\ 0 & 0 & 0 & -1 & 1 & -1 & 2 & 0 & 1 & -1 & 0 & 0 \\ 0 & 0 & -1 & 0 & 0 & 1 & 0 & 2 & 0 & 0 & -1 & 0 \\ 0 & 0 & 0 & -1 & 0 & -1 & 1 & 0 & 2 & 0 & 1 & -1 \\ 0 & 0 & 0 & 0 & -1 & 0 & -1 & 0 & 0 & 2 & 0 & 1 \\ 0 & 0 & 0 & 0 & 0 & 0 & 0 & -1 & 1 & 0 & 2 & -1 \\ 0 & 0 & 0 & 0 & 0 & 0 & 0 & 0 & -1 & 1 & -1 & 2 \end{bmatrix}} \begin{matrix} \\ \\ \\ \\ \\ \\ \\ \\ \\ \\ \\ \\ \end{matrix} \overset{\uparrow}{\underset{\downarrow}{NF}} \tag{36}$$

Note that the structure of this coefficient matrix is very similar to the structure of the cross-flow coefficient matrix contained in the COBRA-IIIC code. The primary difference is that the coefficient matrix used by the code is modified by the addition of the diagonal terms in Eq. (31):

$$\left[\frac{1}{\Delta t}\right] + \left[\frac{u_j^*}{\Delta x}\right] + \left(\frac{s}{l}\right)[C_j] \quad . \tag{37}$$

This modification generally improves the numerical properties of the matrix, and in many cases, provides the diagonal dominance necessary to guarantee the success of iterative solution techniques. However, the iteration is relatively slow to converge, and is not much more efficient from a computational point of view than Gaussian elimination, particularly for problems that involve a moderate number of computational cells. For this reason, the cross-flow distribution is found in COBRA-IIIC by solving Eq. (30) by Gaussian elimination, and it is the repeated application of this inversion technique to Eq. (30) at each axial level of the core at each instant of time that is primarily responsible for the long running time of the code.

For the newly proposed method, the coefficient matrix governing the pressure distribution can be written as

$$[I + \theta M_j] \quad . \tag{38}$$

Since $[I]$ is the identity matrix and $[M_j]$ is defined by Eq. (23), the structure of this coefficient matrix is determined primarily by the order of multiplication of $[S]^T$ and $[S]$. Again, it should be recognized that $[A_j]$, $[u_j^*]$, and $[D_j]^{-1}$ in Eq. (23) are diagonal matrices. Taking the expressions for $[S]^T$ and $[S]$ given previously and multiplying them together in the proper order gives

$$[S]^T[S] = \begin{bmatrix} 2 & -1 & 0 & -1 & 0 & 0 & 0 & 0 & 0 \\ -1 & 3 & -1 & 0 & -1 & 0 & 0 & 0 & 0 \\ 0 & -1 & 2 & 0 & 0 & -1 & 0 & 0 & 0 \\ -1 & 0 & 0 & 3 & -1 & 0 & -1 & 0 & 0 \\ 0 & -1 & 0 & -1 & 4 & -1 & 0 & -1 & 0 \\ 0 & 0 & -1 & 0 & -1 & 3 & 0 & 0 & -1 \\ 0 & 0 & 0 & -1 & 0 & 0 & 2 & -1 & 0 \\ 0 & 0 & 0 & 0 & -1 & 0 & -1 & 3 & -1 \\ 0 & 0 & 0 & 0 & 0 & -1 & 0 & -1 & 2 \end{bmatrix} \quad \begin{matrix} \longleftarrow NP \longrightarrow \\ \\ \\ \\ \\ \\ \\ \\ \\ \end{matrix} \quad \begin{matrix} \uparrow \\ \\ \\ \\ \\ \\ \\ \\ \downarrow \end{matrix} NP \quad . \tag{39}$$

Thus, it can be seen that the coefficient matrix governing the pressure field has an elliptic character, which suggests that the radial pressure distribution obeys a type of Poisson equation. This is a consequence of the fact that the solution scheme is formulated to take advantage of the "primitive variables" governing the flow field, and one of them is the pressure $\{P_i\}$. Furthermore, since the diagonal entries in Eq. (39) are equal in magnitude and opposite in sign to the sum of the off-diagonal entries in any row or column, the matrix has a much simpler and more predictable band structure than that of Eq. (36). This numerically desirable feature stems from the fact that each computational cell in the transverse plane at which the pressure is to be found is only connected to its nearest neighboring cells, whereas in COBRA-IIIC, the cross flow across one boundary may be affected by the cross flow across as many as six other boundaries in the lattice of cells shown in Fig. 1. Thus, it can be seen that the band width of the coefficient matrix is reduced by approximately a factor of 2 if a pressure-based solution scheme is used.

The primary computational advantage of the proposed method lies in the fact that the coefficient matrix governing the pressure field, Eq. (38), is a Stieltjes matrix; that is, the matrix is a diagonally dominant, irreducible, positive definite matrix with a simple and predictable band structure for any nontrivial space-step and time-step size. For consistent numbering schemes, the convergence of standard iterative solution techniques for matrices of this type can be guaranteed. Consequently, it is possible to find the pressure distribution in the lattice by iterative methods rather than by Gaussian elimination. It should be recognized that this has a strong impact on the overall effectiveness of the method, as shown in greater detail in Sec. V.

IV.F. Stability Considerations

For the full potential of the method to be realized, some general guarantee of stability must be given to govern the blending of the pressure fields from adjacent transverse planes as the numerical scheme marches downstream in the axial direction. While it is relatively easy to show that the method is unconditionally stable with respect to the propagation of errors in the transverse direction,[15] it has not yet been possible to develop a general stability criterion for the method when the interaction of the axial direction with the transverse direction is taken into account.

However, a very comprehensive set of numerical tests has been performed to simulate operational reactor conditions, and these tests appear to indicate that the method is stable for all spatial differencing schemes in which θ is taken to be greater than or equal to 0.5. Setting $\theta \geq 0.5$ is

[15]R. E. MASTERSON, "COBRA-IIIP/MIT: An Improved Computer Code for the Multidimensional Thermal-Hydraulic Analysis of Fuel Pin Bundles and Nuclear Reactor Cores," PhD Thesis, Massachusetts Institute of Technology (to be published).

equivalent to requiring that the pressure field that drives the cross-flow distribution must be at least as implicit as the pressure field obtained by taking the average of the pressure distributions that exist at the top and the bottom of each plane of computational cells. Mathematically, this is equivalent to requiring the stability of the Crank-Nicholson method, Eq. (27). More implicit spatial differencing schemes have always been found to be stable.

As far as the temporal differencing scheme is concerned, it should be pointed out that the method is unconditionally stable since the difference equations governing the temporal behavior of the system are fully implicit.

IV.G. Boundary Conditions

Since the proposed method, as well as other marching methods, solves the conservation equations sequentially rather than simultaneously, the boundary conditions to be satisfied are the inlet enthalpy, the inlet mass flow rate, the inlet pressure, and the inlet cross-flow distribution. Alternatively, the exit pressure may be specified as in COBRA-IIIC, and the inlet pressure level may be "floated" to give a uniform outlet pressure. In either case, the sequential nature of the solution procedure allows arbitrary spatial and temporal forcing functions to be applied to the system pressure, the inlet enthalpy, the inlet mass flow rate, and the radial and axial power distributions. The cross flow at the core inlet is usually assumed to be zero, although more detailed cross-flow distributions may be prescribed if a better physical picture is required and if enough experimental evidence is available to specify it.

It is of major importance to realize that one of the primary differences between the proposed method and that used by the COBRA-IIIC code lies in the treatment of the system pressure. Whereas in the first method the system pressure is fully integrated into the solution scheme because it is used directly in the conservation equations, it is eliminated in the latter in favor of a system of equations based on pressure differences between the computational cells. Both approaches are acceptable under normal operating conditions as long as the pressure is treated consistently and the physical properties of the coolant are evaluated at a reasonable pressure, such as the exit pressure of the system. It should be pointed out, however, that under circumstances where the variation of the saturation temperature with local pressure must be taken into account, the new method of solution has a definite computational advantage, since it works directly with the pressure.

Due to the fact that this method works with a pressure-oriented solution scheme, it is possible to specify an inlet pressure distribution together with an inlet mass flow distribution. However, this boundary condition has not yet been fully integrated with the proposed solution scheme.

IV.H. Convergence Behavior

The convergence of marching-type methods such as those described above is usually achieved by sweeping downstream several times in succession and by iterating on the flow distribution until the change in the mass flow rate formed from successive axial iterations is less than some prescribed convergence criterion. In practice, it is important to realize that axial iterations after the first usually contribute to only minor changes in the flow distribution but consume a great deal of additional computational time, since it is necessary to completely recompute the cross-flow distribution every time a new axial iteration is performed; consequently, care should be exercised in selecting a reasonable convergence criterion. For example, it makes no sense to iterate on a very tight convergence criterion if the accuracy of the solution is already in question in the first or second decimal place. This is particularly true in situations where the magnitude of the cross flow at any point along the length of a channel is >5 or 10% of the axial mass flow rate. Moreover, it has been found that very little can be gained from a practical point of view by converging the axial mass flow rate to more than *two* decimal places in most problems, since the uncertainties in the empirical correlations employed are at least as great as the errors inherent in the physical model used by the method itself.

Therefore, it is strongly recommended that users of either method take these factors into consideration when attempting to select a reasonable value for the flow convergence criterion.

IV.I. The Axial Iteration Scheme

Many thermal-hydraulic analysis codes[3,7,9] are based on an axial iteration scheme that consists of sweeping downstream between the inlet and outlet of the core several times in succession and iterating on the flow distribution until the difference between the mass flow rates formed from successive axial iterations is less than some prescribed convergence criterion. In practice, procedures of this type can be extremely inefficient from a computational point of view because they require the cross-flow distribution to be completely recomputed over the entire axial height of the core, although there may be only one or two points (out

of several thousand in some cores) where the cross-flow distribution may initially fail to converge.

For the new method of solution, this shortcoming has been overcome by adopting an iteration scheme in which additional iterations are performed at only those points in the lattice where they are needed. This iterative scheme consists of solving Eq. (22) for the pressure field and then solving Eq. (29) for the cross-flow distribution to complete the first iteration. If the change in the axial mass flow rate from the bottom to the top of a node is less than some prescribed convergence criterion, the flow field is assumed to converge, and the numerical method is allowed to sweep downstream to the next axial level. If, however, the flow field has not converged, an entirely new iterative scheme is constructed for use with subsequent iterations. This scheme consists of substituting the most recent values for the cross-flow and axial mass flow distributions back into the axial momentum equation, Eq. (8), to generate a new pressure field $\{P_j\}'$ at the top of the node. This pressure field is then blended together with the pressure field from the bottom of the node $\{P_{j-1}\}$ to form the composite pressure field given by Eq. (9). After the transverse momentum equation has been solved for the cross-flow distribution $\{w_j\}'$ that results from the application of this pressure field, the continuity equation, Eq. (6), is solved for a new axial mass flow distribution, $\{m_j\}'$. If the flow field has not converged, these values are fed back into the axial momentum equation to generate a new pressure field, $\{P_j\}''$, and another iteration is performed. This process is repeated several times in succession until the flow field appraoches an asymptotic value. In this case, it is assumed that the iteration has converged, and the numerical method is allowed to sweep downstream to the next axial level. This scheme has the advantage that it eliminates the need to solve Eq. (22) or (30) more than once, while it uses information gained from the first iteration to reduce the complexity of subsequent steps in the iterative process. This saves an enormous amount of computation time compared to other iterative schemes and enables problems to be solved with much larger numbers of computational cells.

In some cases, convergence of the iteration can be accelerated by modifying the newly computed values of $\{P_j\}$ and $\{w_j\}$ according to the algorithms

$$\{P_j\}^n = \alpha\{P_j\}^n + (1 - \alpha)\{P_j\}^{n-1} \tag{40}$$

$$\{w_j\}^n = \beta\{w_j\}^n + (1 - \beta)\{w_j\}^{n-1} \tag{41}$$

where n is an iteration index and α and β are free parameters analogous to relaxation factors. Although $\alpha = \beta = 1.0$ is usually sufficient, smaller values have been found to accelerate the convergence of some problems.

Finally, it should be pointed out that the cost of the first (and usually the most expensive) iteration can be reduced considerably by obtaining a good estimate of the pressure distribution before solving Eq. (22) by iterative means. This can be achieved for operational reactor conditions by setting

$$\{P_j\} = \{P_{j-1}\} + \left(\frac{\partial P}{\partial x}\right)_o \cdot \Delta x \quad , \tag{42}$$

where

$$\left(\frac{\partial P}{\partial x}\right)_o$$

is the pressure gradient due to frictional and gravitational effects. With this assumption, it is usually possible to converge the pressure vector in Eq. (22) to 3 or 4 decimal places in ~10 radial iterations using either the method of successive overrelaxation on a pointwise basis or a cyclic Chebychev iterative technique.

IV.J. Conservation of Energy

The purpose of the preceding discussion has been to develop a general numerical method for solving the equations for the conservation of mass and momentum in fuel pin bundles and nuclear reactor cores. The energy equation, Eq. (2), was not considered explicitly because an understanding of its structure was not necessary for the development of the proposed method. However, after the equations for the conservation of mass and momentum have been solved, the thermal response of the fluid must be interfaced with the hydraulics through heat transfer coefficients. This is generally done by solving the energy equation, Eq. (7), for the enthalpy of the fluid at a new axial level, h_j, using the value of the enthalpy from the previous axial level, h_{j-1}, and the rate of energy generation known to exist in each computational cell. The energy balance is performed using the axial mass flow rates, $\{m_j\}$, found from a previous solution of the momentum equations. Thus, the solution of the energy equation can be looked upon as an "outer iteration" in the two-step solution procedure. Generally speaking, it is necessary to iterate between the energy equation and the momentum equations at least once at each axial elevation to obtain a self-consistent solution to the entire system of conservation equations. For problems that involve considerable departures from operational reactor conditions (i.e., moderately severe transients), additional interactions

between the energy equation and the momentum equations may have to be performed.

V. THE COBRA-IIIP/MIT CODE

The numerical method developed in this paper has been built into a new production code called COBRA-IIIP/MIT, which yields satisfying solutions to a wide variety of practical problems under operational reactor conditions. The code is based on the same physical formalism as the COBRA-IIIC code, but due to improvements in the method of coding and the numerical solution scheme used, it is possible for the code to handle extremely large and complex problems with great speed. For example, the code is capable of solving problems with as many as 625 channels with arbitrary geometrical shapes. There is no limit to the number of time steps and space steps that can be used by the code. The code can accept arbitrary radial and axial heat flux distributions as well as all the boundary conditions originally contained in COBRA-IIIC. One of the major innovations incorporated into the COBRA-IIIP/MIT code is a dynamic data management subroutine that allows the dimensions of the principal arrays as well as the total storage requirements to be a function of the size of the problem being solved.

To more clearly comprehend the capabilities of the new code as well as its intended range of applicability, it is important to understand the types of problems to which the code can be applied. This generally includes all problems encountered during operational reactor conditions, including transients in which simultaneous changes in the system pressure, the heat generation rates, and the inlet mass flow rates must be taken into account. It should be recognized that the code is *not* designed nor is ever intended to be used to analyze the effects of severe blockages and flow reversals, although there is a possibility that the code will yield self-consistent solution to a problem in which there is a small flow blockage. Finally, it must be understood that the correlations for the void fraction and critical heat flux ratios used by the code are most accurate for the qualities and heat flux ratios usually encountered during the operation of a pressurized water reactor. They become less valid at higher qualities and for highly nonuniform heat fluxes; consequently, results should be interpreted with care in these cases.

Table I gives a comparison of the computation time needed by the various codes to compute the cross-flow distribution as a function of the number of computational cells. It can be seen in all cases that the COBRA-IIIP/MIT code is considerably faster and more efficient than its predecessors. Whereas the cross-flow computation time of the COBRA-IIIC code increases as the number of cells cubed, and the cross-flow computation time of COBRA-IIIC/MIT still increases as the 1.6 power of the number of cells, the computation time required to compute the cross-flow distribution with COBRA-IIIP/MIT is approximately a linear function of the number of cells. It should be noted that the results in Table I are given for one axial iteration. In practice, all these codes require several iterations to converge to a self-consistent flow distribution; however, the time required by COBRA-IIIP/MIT to perform these iterations is considerably less due to the use of the more efficient axial iteration scheme outlined in Sec. IV.I. This usually reduces the computation time by an additional factor of 3 or 4 compared to the other two codes, depending on the type of problem being solved. The total execution time of the COBRA-IIIP/MIT code is 70 or 80% greater than the cross-flow solution times shown in Table I. This appears to indicate that the code is considerably more efficient and powerful than its predecessors.

TABLE I

A Comparison of Cross-Flow Solution Times* (in seconds)

Number of Channels	16	64	128	200	300	400
COBRA-IIIC	1.71	128.49[a]	987.36[a]	3293.61[a]	10 250.00[a]	31 980.00[a]
COBRA-IIIP/MIT	0.14	0.42	1.23	1.78	2.65[a]	3.59[a]
COBRA-IIIC/MIT	0.17	1.38	9.09	19.67	39.80[a]	81.24[a]

*All results are for ten axial levels on an IBM 370/165 with the *H* compiler. Note that the results of these timing runs may vary by ±10% during the course of a day due to changes in the work load on the system.

[a]For economic reasons, these results are estimated by extrapolation.

VI. RESULTS

In the following discussion, two sample problems are presented in which the results of the COBRA-IIIP/MIT code are compared to those of COBRA-IIIC/MIT (e.g., COBRA-IIIC).

The lattice of sample problem I is shown in Fig. 2, and the input data for this case are given in Table II. The results illustrated in Fig. 3 show that the COBRA-IIIP/MIT code gives a departure from nucleate boiling ratio (DNBR), which is consistently 2 or 3% higher than that given by COBRA-IIIC/MIT. This may be significant because it indicates that it may be possible to recover a small amount of the total operational power under certain types of conditions.

Moreover, Fig. 3 shows that the Westinghouse (W-3) correlation gives a more conservative estimate of the DNBR than the Babcock and Wilcox (B&W-2) correlation over the whole axial length of the core. Note that the two correlations deviate from one another by as much as 20% in the hottest region of the channel for the given input parameters.

Figure 4 shows a much simpler lattice used for sample problem II. The input data are summarized in Table III. A grid with a loss coefficient of 2.5 is located midway between the inlet and the outlet of the core and is assumed to extend over the whole lattice. In this case, a single computational cell is used to represent an entire fuel pin assembly, and the power level in all the assemblies in the core is increased uniformly by a factor of 2 in 2 s.

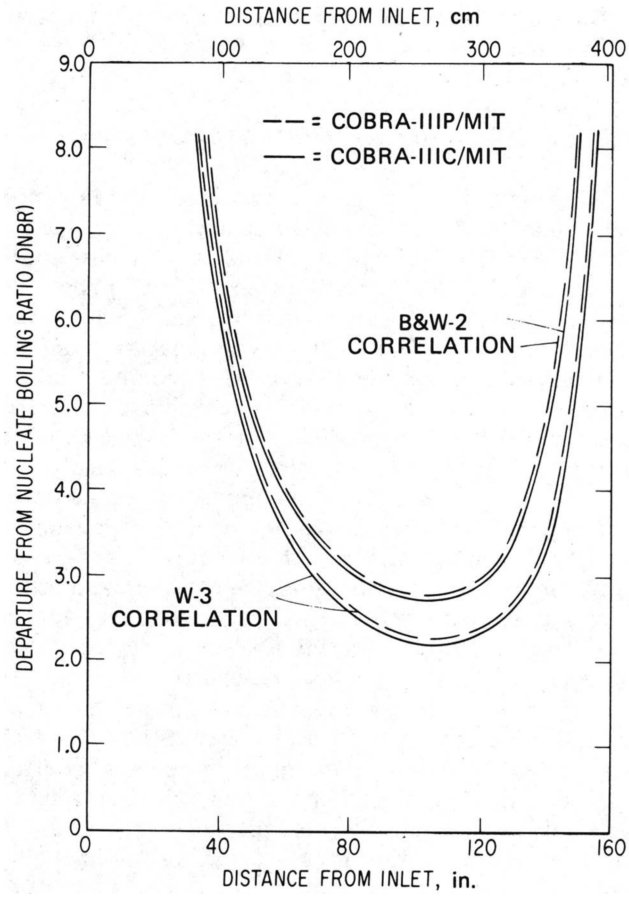

Fig. 3. Axial distribution of DNBR for the hottest rod of sample problem I as shown in Fig. 2.

TABLE II

Input Parameters for Sample Problem 1

Type of Reactor—Pressurized Water	
Axial power distribution—skewed cosine	
Radial power peaking factors as shown	
Nominal operating conditions:	
System outlet pressure:	2100 psia
Inlet temperatures (uniform for all channels):	541.0°F
Average inlet mass flux (uniform for all channels):	2.51×10^6 $lb_m/(h\ ft^{-2})$
Average reactor heat flux:	0.21×10^6 $Btu/(h\ ft^{-2})$
Axial mesh spacing:	6 in.
Channel length:	180 in.

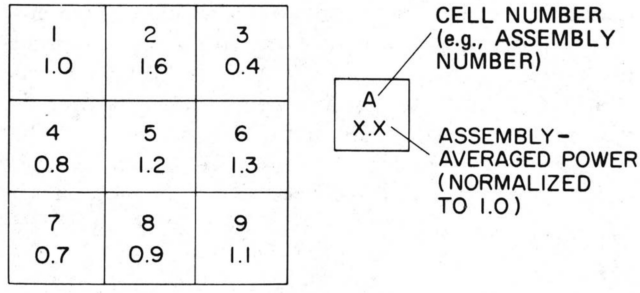

Fig. 4. Sample problem II—a simple bundle configuration for numerical testing.

Figures 5a and 5b, as well as Figs. 6a and 6b, show that both codes are in reasonably good agreement with one another at the beginning of the transient, since both predict approximately the same magnitude and shape for the cross-flow distribution between assemblies 2 and 3 and the same axial mass flow rate in assembly 2. However, at t = 1.0 s, considerable differences begin

to develop between the predictions of the two codes. One of the primary differences is that the COBRA-IIIC/MIT code (i.e., COBRA-IIIC) apparently no longer "sees" the grid, whereas Fig. 5b clearly depicts that the effects of the grid (as predicted by COBRA-IIIP/MIT) are even more pronounced. This is probably due to the fact that the new code is more accurate in predicting changes in the pressure fields in the vicinity of the grid. However, these effects are not strong enough to show up in the plots of the axial mass flow distribution shown in Figs. 6a and 6b.

TABLE III

Input Parameters for Sample Problem 2

Type of Reactor—Pressurized Water	
Axial power distribution—uniform	
Radial power peaking factors as shown	
Nominal operating conditions:	
System outlet pressure:	2100 psia
Inlet enthalpies (uniform for all changes):	538.0 Btu/lb_m
Average inlet mass flux (uniform for all channels):	2.48×10^6 $lb_m/(h\ ft^{-2})$
Average reactor heat flux:	0.2×10^6 $Btu/(h\ ft^{-2})$
Channel length:	120 in.
Axial mesh spacing:	2 in.
Flow area for each cell:	0.266 ft^2
Number of rods per cell:	225

The onset of bulk boiling is accompanied by a remarkable increase in the cross-flow distribution. The two codes predict different locations for the onset of bulk boiling, as well as somewhat different magnitudes and shapes for the cross-flow distributions during the transient. These factors have a significant effect upon the axial mass flow distributions shown in Figs. 6a and 6b. The difference in the predicted axial mass flow rates at the outlet of the hot assembly are ~1% at $t = 0$, 7% at $t = 1$ s, and 10% at $t = 2$ s for this particular problem. The mass flow rate does not change at the inlet of the lattice because it is a fixed boundary condition.

Based on the results that have been presented here as well as other test cases that have been run, it has been found that the predictions of the two codes are in reasonable agreement with one another as long as they are used to analyze operational reactor conditions. However, the results of the two codes differ from one another primarily in their predictions of the flow distributions at the

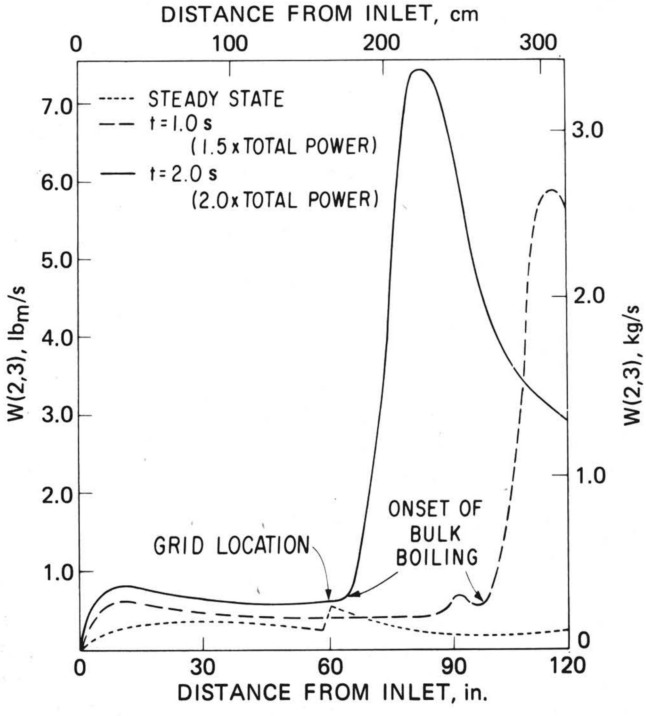

Fig. 5a. Cross flow between assemblies 2 and 3 in sample problem II as predicted by COBRA-IIIC/MIT.

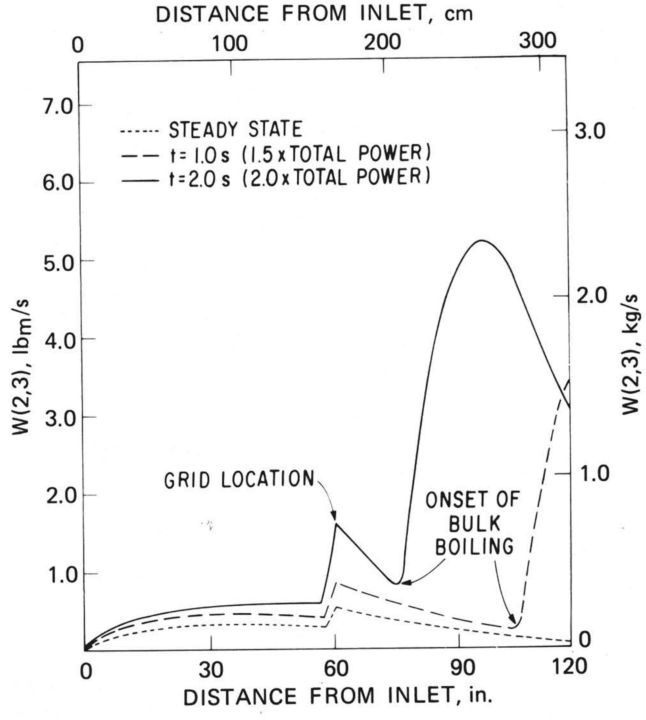

Fig. 5b. Cross flow between assemblies 2 and 3 in sample problem II as predicted by COBRA-IIIP/MIT.

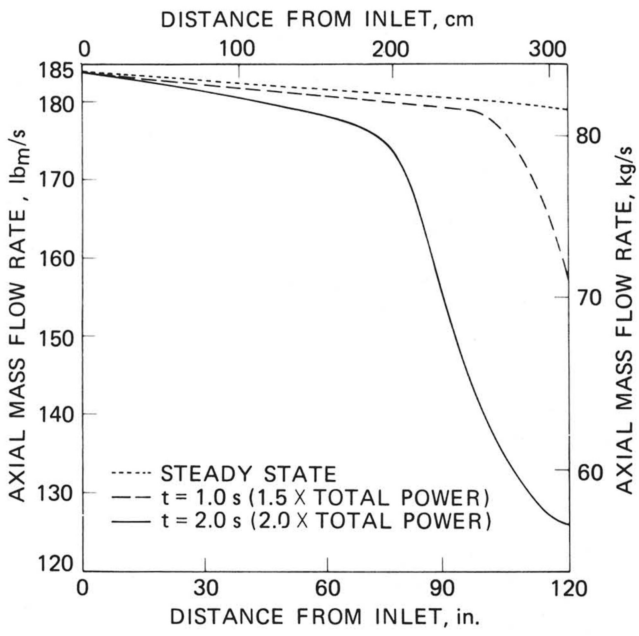

Fig. 6a. Axial mass flow rate in assembly 2 as predicted by COBRA-IIIC/MIT.

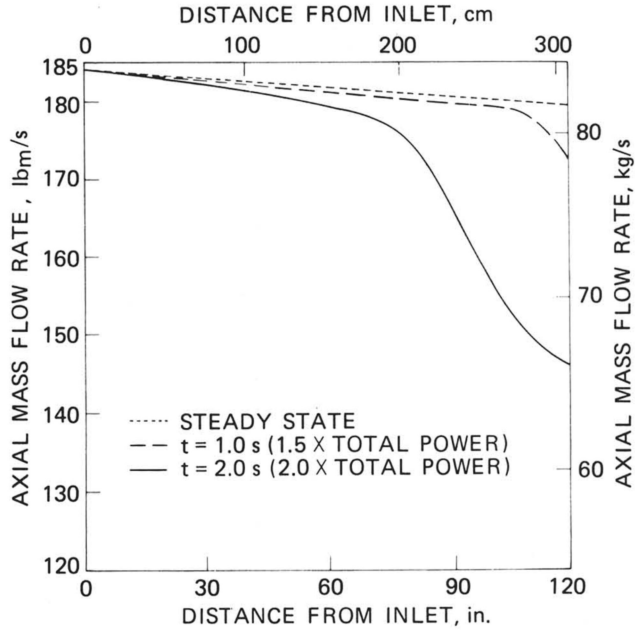

Fig. 6b. Axial mass flow rate in assembly 2 as predicted by COBRA-IIIP/MIT.

reactor inlet, in regions of strong boiling, and in the vicinity of rod spacers (e.g., grids). These differences do not appear to be important for steady-state conditions, although they become larger and more significant when the codes are used to model severe transients where the effects of simultaneous changes in the mass flow rates and power levels must be taken into account. It is strongly recommended that experiments be performed to determine the flow distributions between rod bundles during transient conditions, so that a meaningful comparison of the predictions of the codes and their capabilities can be made. However, it is believed that the new code appears to give a more detailed and consistent physical picture of what one would expect to happen when it is applied to certain types of simple problems.

VII. CONCLUSIONS

In conclusion, it can be seen that the success of a complex computer code depends on many factors. These include the topological layout of the lattice, the form of the conservation equations, and the correlations that are used to interface the thermal response of the system with the hydraulics.

The successful development and application of the COBRA-IIIP/MIT code rely upon the well-balanced integration of all these factors, although the superiority of the solution scheme is also of major importance.

It is felt that the pressure-oriented method of solution presented here is advantageous in cases where the effect of the pressure on the saturation temperature of the coolant must be taken into account. Moreover, this solution scheme may allow more flexible changes to be made in the formulation of the transverse momentum equation without affecting the overall computational efficiency of the method that has been proposed.

With increasing specialization of marching-type, production-oriented, thermal-hydraulic analysis codes, the need will certainly arise to more precisely determine their range of applicability. For this purpose, experiments to simulate time-dependent reactor behavior during both single-phase and two-phase flow conditions should be performed.

It is recognized that the methodology developed here can be applied equally well to analyze the steady-state and transient behavior of liquid-metal fast breeder reactor cores. This entails the development of reasonably efficient topological layouts and cell numbering schemes to deal with the hexagonal arrays encountered in these systems.

Thus, it can be seen that the COBRA-IIIP/MIT code and the numerical method on which it is based are extremely efficient and powerful tools for use in coupled-neutronic-thermal-hydraulic calculations, on-line reactor simulations, and in the generation of response surfaces using the methods of experimental design.